Available online at www.sciencedirect.com
SCIENCE DIRECT®
Renewable Energy 29 (2004) 823–839
RENEWABLE ENERGY
www.elsevier.com/locate/renene

Microstructural optimization and extended durability studies of low-cost rough graphite–aluminium solar absorber surfaces

P. Konttinen *, P.D. Lund

Advanced Energy Systems Laboratory, Helsinki University of Technology, P.O. Box 2200, 02015 HUT, Finland

Received 1 August 2003; accepted 20 November 2003

Abstract

Mechanically manufactured low-cost selective inhomogeneous rough graphite–aluminium ($C/Al_2O_3/Al$) solar absorber surfaces provide, at the current state of development, solar absorptance $\alpha = 0.90$ and thermal emittance $\varepsilon = 0.22$. Based on a literature review, significantly lower emittance values could theoretically be achieved by utilization of surface plasmons in rough surfaces with an optimal graphite layer thickness, groove depth and sinusoidal surface profile periodicity. It is possible that an arbitrary form of roughening could produce equally good optical properties. In order to achieve lower emittance manufacturing parameters, the composition of silicon carbide grinding pad and the corresponding grinding pattern are required to be enhanced. The commercially available grinding pads used so far have not yielded optimal results. An antireflection coating could improve α to >0.90. Absorber samples were subjected to 383 days of temperature and irradiance cycling. In total, the samples were exposed to ultraviolet (UV) irradiation equivalent to 5–15 years of normal outdoor use. The results show that the samples are not sensitive to natural levels of UV irradiation or cycling-induced degradation of optical properties. A clear increment in absorptance was observed after the first 50 days of cycling. The elevated temperature of 130 °C is the probable cause for the increase. Reference samples indicated similar aging behaviour both after 4 years of natural exposure and after relatively short constant temperature tests at 120 and 180 °C.

Keywords: Rough solar absorber surface; $C/Al_2O_3/Al$; Mechanical manufacturing; Surface plasmons; Cyclic aging

* Corresponding author. Tel.: +358-9-4513212; fax: +358-9-4513195.
E-mail address: petri.konttinen@hut.fi (P. Konttinen).

0960-1481/$ - see front matter © 2004 Elsevier Ltd. All rights reserved.
doi:10.1016/j.renene.2003.11.008

1. Introduction

Spectrally selective solar absorbers are used for efficient conversion of solar energy to heating energy, e.g. for domestic hot water. State-of-the-art absorbers have good durability and excellent optical properties: solar absorptance α is close to unity and thermal emittance ε is close to zero. The downside is the typically quite high cost of such absorbers due to the costs of the manufacturing technology, typically sputtering. For certain applications such as swimming pool heating, lower cost absorbers having lower efficiency can be used. One method to produce a low-cost absorber with reasonable efficiency is mechanical manufacturing.

The $C/Al_2O_3/Al$ absorber coating contains an inhomogeneous rough graphite–alumina groove matrix on an Al substrate. The coating is mechanically manufactured on an Al-sheet by single phase grinding with a silicon carbide grinding pad [1]. During grinding, the naturally formed Al_2O_3 layer on the surface of the Al substrate increases as well [1,2]. The whole process for a $2 \times 0.12 \times 0.005$ m^3 Al-sheet lasts for about 15 min at the present stage of development and does not produce any toxic waste. The manufacturing unit can be duplicated inexpensively, thus enabling simultaneous production of multiple absorber sheets. A solar absorptance $\alpha = 0.90$ and a thermal emittance $\varepsilon = 0.22$ have been achieved so far [2]. Previous studies of solar absorbers combining a graphite layer and a rough surface have been published in the late 1970s [3,4]. Another early work [5] has been published about using mechanical grinding to increase the selectivity of surfaces prior to deposition of a multilayer interference coating. The mechanical manufacturing method differs from these in that it utilizes grinding for forming the selective surface without any other further treatments. The main concept is to roughen the Al surface and mechanically add a graphite layer on it simultaneously.

A service lifetime of at least 25 years is a commonly used design target for solar absorbers. In order to determine the estimated service lifetime of an absorber, series of accelerated aging tests are normally carried out. The IEA solar heating and cooling programme (IEA SHC) has proposed an accelerated aging test procedure as a standard to ISO TC 180 "Solar Energy" (draft ISO/DIS 12592) [6–9]. The standard tests were originally designed for the qualification of electroplated and sputtered selective absorber coatings. If a surface contains an organic coating, the effect of ultraviolet (UV) degradation on the optical performance should be considered as well [8]. In addition, the performance of selective absorbers can be degraded by poor film adhesion during thermal cycling over large temperature ranges [3].

In order to determine the sensitivity of the $C/Al_2O_3/Al$ surface coating to ultraviolet–visible–infrared (UV–Vis–IR) irradiance and temperature cycling, absorber samples were subjected to cycling under different irradiance levels. Standard IEA SHC test results for high temperature and combined elevated temperature and high humidity/condensation will be published separately [10]. Those results indicate that the absorber coating shows no deterioration in optical properties at high operation temperatures (200 h at 250 °C). The main degradation mechanism is found to be hydration of aluminium oxide to pseudoboehmite and boehmite. The hydration process accelerates according to the Arrhenius relation as the temperature rises

with the presence of condensed water on the surface. High humidity alone without condensation is significantly less harmful. The estimated time of normal use is 20–25 years before the energy yield of the solar collector has decreased by 5%. The conclusion is that the $C/Al_2O_3/Al$ absorber coating passed the IEA SCHP standard tests for temperature and moisture load.

2. Optimization of microstructure of $C/Al_2O_3/Al$ surface based on literature review

Detailed optical and microstructural analyses of the $C/Al_2O_3/Al$ surface are given in [1,2]. Fig. 1 (left) shows an example of how the microgrooves are organized on the surface. In Fig. 1 (right) can be seen graphite clusters of varying thickness (dark areas) and the uncovered Al_2O_3 surface (light areas). Fig. 2, which has been extracted from the background of a crosscut scanning electron microscopy (SEM) micrograph [2] shows an approximate example of the surface profile and graphite cluster size and distribution.

Botten and Ritchie [3] have theoretically calculated optimal parameters for a solar absorber surface based on diffraction gratings embodied in thin film interference systems. They studied single dimensional uniform sinusoidal profile graphite–copper interfaces by altering the mean thickness of the graphite layer, the period of the surface modulation and the depth of the roughening. By using periodic surfaces, they could utilize a grating absorption phenomenon known as surface plasmons for eliminating the deleterious absorption minimum of the graphite. A detailed description of surface plasmons on rough surfaces can be found in [11]. These plasmons are excited on the long wavelength side of Wood anomalies [12] ($\lambda = D/n$; D is the grating period and n is an integer) and are determined by the shape of the roughened surfaces and the optical properties of the medium surrounding the interface. Botten and Ritchie [3] aimed to excite a surface plasmon centred on the absorption minimum at approximately 0.6 μm and therefore used a grating period of 0.5 μm in order to station a Wood anomaly at a wavelength of

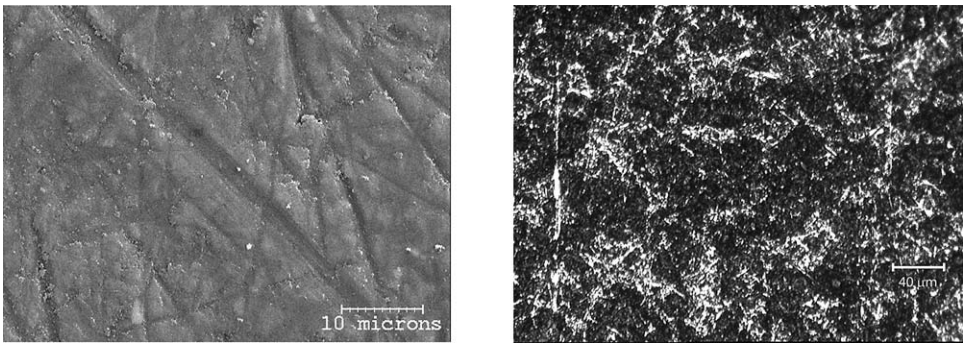

Fig. 1. Scanning electron micrograph (left) and optical microscope photograph (right) of two typical $C/Al_2O_3/Al$ surface samples.

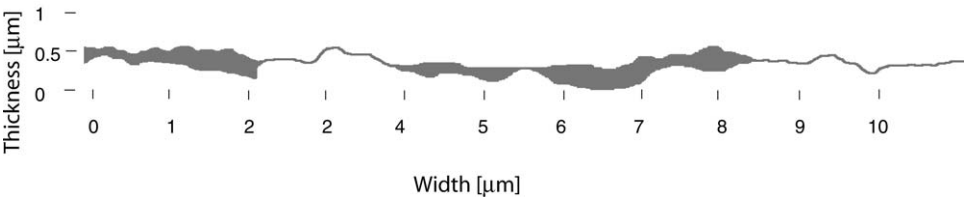

Fig. 2. Approximation of a $C/Al_2O_3/Al$ surface profile and graphite cluster size and distribution. The profile has been extracted from a crosscut SEM micrograph [2]. The maximum visible graphite cluster thickness is in the range of 0.3 μm.

0.5 μm. They calculated that an optimized diffraction grating would have $\alpha = 0.884$ and $\varepsilon = 0.062$ (mean graphite thickness 0.12 μm, depth of roughening 0.15 μm and roughness period 0.5 μm). Based on the results achieved, they predicted that an arbitrary form of roughening would produce results similar to those for sinusoidal form.

Botten and Ritchie [3] have also compared the performance of a roughened surface with that obtained by grading the refractive index of the absorber and noticed that refractive index grading tends to smoothen the entire absorption spectrum by removing any deep absorption minima coinciding with the peak of the solar spectrum for the sinusoidal graphite layer. In addition, they calculated α and ε for various plane uniform graphite film thicknesses. For a thickness of 0.4 μm, they calculated $\alpha = 0.86$ (unspecified air mass (AM)) and $\varepsilon = 0.41$ (at 700 K). A thickness of 0.3 μm gave $\alpha = 0.85$ and $\varepsilon = 0.25$.

Golomb [4] has experimentally studied graphite–copper interference films, which were deposited by electron beam evaporation on holographically produced diffraction gratings and meshes. He noticed a strong plasmon effect raising α from 0.79 to 0.88 while leaving ε constant at 0.04. The parameters used were: roughness period of 0.642 μm, graphite thickness of 0.12 μm and groove depth of 0.17 μm (Fig. 3). Compared to a plane interface with the same graphite thickness the solar reflectance was approximately halved, while ε was increased by <0.01. His experience was that biperiodic graphite–copper surfaces had a slightly greater absorptance than uniperiodic surfaces. This feature implied that a randomly roughened surface might be even more absorbing than the corresponding uniperiodic surface, which is in accordance with the results of Botten and Ritchie [3].

McKenzie [13] has studied the effect of substrate on graphite selective surfaces. He determined that at operation temperatures below 100 °C, copper, silver and nickel are almost equally good candidates for metal substrates. However, the graphite layer thickness required to yield the most available power varied significantly from 0.317 μm for Cu and Au to 0.163 μm for Ni. Based on these results it is uncertain whether the thicknesses obtained by Botten and Ritchie [3] and Golomb [4] for graphite–copper interfaces are directly applicable to the mechanically manufactured graphite–aluminium surfaces.

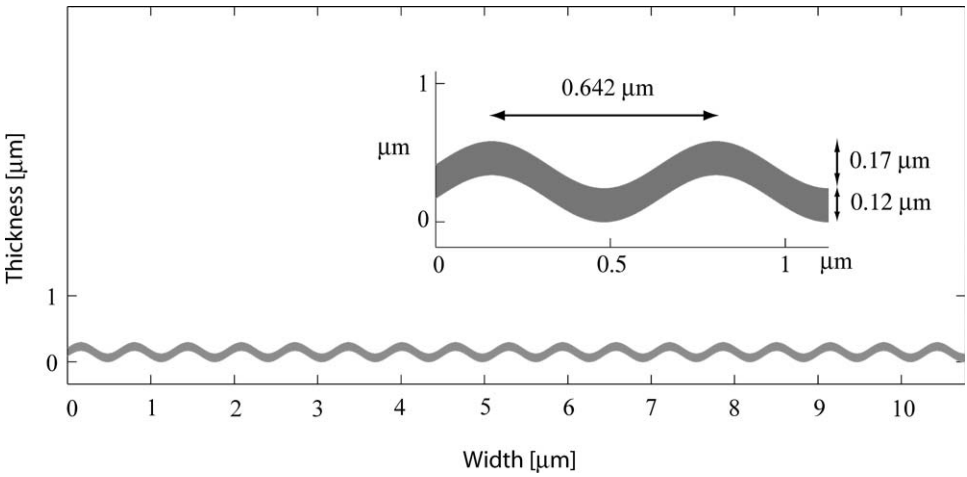

Fig. 3. Optimal surface profile parameters for a roughened sinusoidal graphite–copper diffraction grating thin film interference solar absorber according to Golomb [4]. Roughness period 0.642 μm, graphite thickness 0.12 μm and groove depth 0.17 μm.

The graphite film of the $C/Al_2O_3/Al$ surfaces is not uniformly thick and covering, nor does it form a sinusoidal profile (Figs. 1 and 2). Comparison of the values of optical properties obtained by Botten and Ritchie [3] and Golomb [4] to those obtained by Konttinen et al. [1,2] indicate that the $C/Al_2O_3/Al$ surfaces do exhibit optical properties similar to some extent despite different profiles (Figs. 2 and 3). The best of the $C/Al_2O_3/Al$ surfaces optically exceeds reference films with a plane graphite film thickness of 0.3–0.4 μm [3], thus indicating that some surface plasmon excitation may occur.

The manufacturing parameters of the $C/Al_2O_3/Al$ surface should be altered to produce surfaces close to that recommended by Botten and Ritchie [3] and Golomb [4] (Fig. 3). This would require optimization of composition of the grinding pad and the grinding pattern, as the commercially available grinding pads tested so far do not seem to allow optimized surface topology to be formed [2]. By adding an antireflection coating, the α of the optimized surface could increase to over 0.90 with the ε unaffected. A low-cost option could be colloidal silica dipping AR-coating [14].

3. Cycling and constant temperature test procedures

Temperature and irradiance cycling tests were performed using a climate chamber, model Arctest ARC 400. The test method and equipment are described in detail in [15]. Fig. 4 shows an overview of the inner chamber of the climate chamber together with the UV-lamps and sample holder used for phase 3 testing. Phase 2 was similar, except that the lamps were oriented vertically and the samples hori-

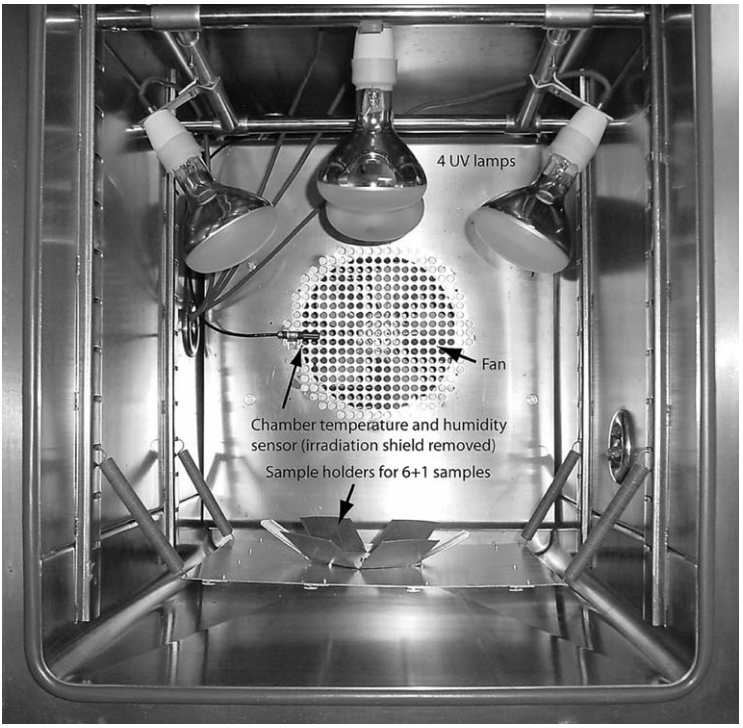

Fig. 4. Photograph of the test chamber showing the principle of phase 3 testing (reconstructed). Inner chamber dimensions $0.59 \times 0.8 \times 0.75$ m^3, volume 354 l. Six samples (7 cm × 7 cm) can be tested simultaneously at a 30° slope inclination. One sample can be tested in the middle of the sample holder with approximately 75% higher irradiance.

zontally. For phase 1, an external solar simulator was used and the samples were oriented vertically.

Solar absorptance (AM 1.5) was determined between 0.39 and 1.1 μm with a Li-cor LI-1800 spectroradiometer and an integrating sphere. Thermal emittance (at 100 °C) was determined between 2.5 and 20 μm with a Midac Prospect type Fourier Transform IR (FTIR) spectrometer with a semi-integrating device. Comparative measurements for unaged and 383 days aged samples were performed at the Ångström laboratory of Uppsala University. Their equipment consists of a Beckman 5240 spectrophotometer with a $BaSO_4$ integrating sphere for UV–Vis–near infrared (NIR) and a Bomem-Michelson 110 FTIR spectrophotometer with a golden integrating sphere for IR. Absorptance and emittance values of the samples as new and after 383 days of cycling are based on the Uppsala measurements. All the other α and ε values were measured only with Li-cor and Midac, respectively. The irradiance between 0.305 and 2.8 μm at the level of the samples was measured using a Kipp & Zonen CM 11 Pyranometer.

The purpose of the cycling test was to simulate and accelerate the temperature and irradiance conditions that the absorber surfaces are exposed to in normal outdoor use. The upper temperature limit of the chamber was a restrictive factor as the maximum selective $C/Al_2O_3/Al$ absorber surface stagnation temperatures inside a flat plate solar collector can rise up to 180 °C. As the standard tests at 250 °C showed no degradation due to high temperature [10], we considered the maximum available chamber temperature level of 120 °C to be sufficient for the cyclic tests. Additional tests were performed at 120 and 180 °C for determining the effect of constant temperature alone on the optical properties.

3.1. Phase 1, external solar simulator, 1–100 days

Wan et al. [16] performed a cyclic series of constant temperature aging where they exposed absorber samples to 720 h of cycling. We used a cycle of 16 h at 100 °C and 8 h at −40 °C, and repeated this cycle for 100 days. The intervals and temperatures were chosen in order to expose the samples to repetitive irradiation periods with a freezing rest period in between, simulating exaggerated winter conditions in Central Europe. The chamber was operated in conjunction with a solar simulator (model Arrilite AL 2000) during the 16 h at 100 °C period of each 24 h cycle. Nine samples, 10 cm × 10 cm each in a 3 × 3 matrix, were placed vertically inside the chamber. Three of these nine samples were mechanically manufactured selective $C/Al_2O_3/Al$ surfaces, denoted A, B and C. The manufacturing processes and parameters for these samples have been communicated by Konttinen et al. in [1]. The samples were additionally heated up by the solar simulator, but the maximum sample temperature remained below 130 °C (Fig. 5). The total measured irradiance in the middle of the sample matrix varied from 950 to 1200 W

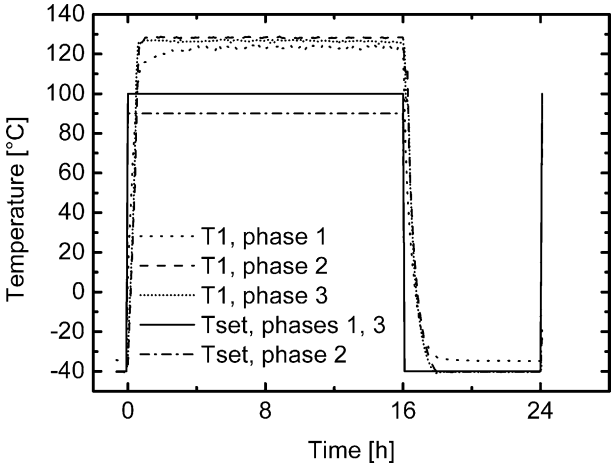

Fig. 5. Typical temperature behaviour during a temperature and irradiance cycling test 24-h sequence. T1 is the thermistor behind sample A; Tset is the chamber temperature set-point. All three test phases showed.

Table 1
UV and total irradiance levels during temperature and irradiance cycling inside the climate chamber for phases 1–3. Results for samples A–C

	Irradiance (W m^{-2})	Sample A	Sample B	Sample C
Phase 1, external solar	UV	2.3	2.0	2.3
simulator, 1–100 days	Total (305–2800 nm only)	840	730	840
Phase 2, vertical UV-lamps,	UV	41	50	46
101–250 days	Total (305–2800 nm only)	1500	1800	1600
Phase 3, single-point-focused	UV	200	110	120
UV-lamps, 251–383 days	Total (305–2800 nm only)	7000	4000	4400

m^{-2} depending on the operation age of the bulb. The irradiance intensity dropped to 600–700 W m^{-2} at the edges of the sample matrix. Samples reported in this paper received an average measured irradiance of 730–840 W m^{-2} (Table 1). We estimate that the total irradiance in the middle of the samples was over 1200 W m^{-2}, a large proportion of it being in the long-wave IR area beyond the measuring range of 305–2800 nm [15]. Aging by solar irradiation is mostly caused by the UV part of the irradiation [17]. Therefore, the long-wave IR irradiation was neglected in the aging effect analysis.

3.2. Phase 2, vertical UV-lamps, 101–250 days

For phase 2, the share of the UV irradiance was increased but the measured total irradiance was kept within the approximate of 1000 W m^{-2}. A four-lamp matrix of UV-lamps (model Osram Ultra-Vitalux) was arranged vertically in the ceiling of the climate to increase the UV irradiance. The aperture of the climate chamber was sealed using steel sheets and adequate insulation material in between. This reduced heat losses, thus resulting in temperature uniformity inside the chamber within 1 °C, as can be seen when comparing temperatures "T1, Phase 1" and "T1, Phase 2" in Fig. 5. Temperature and irradiance cycling was continued for another 150 days with the UV-lamps, similar to phase 1, except that the chamber maximum temperature set-point was lowered down to 90 °C due to the heat load from the UV-lamps to the chamber cooling system. The lamps were on while the temperature set-point of the chamber was 90 °C, i.e. 16 h during every 24 h cycle.

3.3. Phase 3, single-point-focused UV-lamps, 251–383 days

For phase 3, the level of the UV irradiance was increased further. The total irradiance levels were increased to 4000–7000 W m^{-2}. All the four lamps were focused on the middle of a new sample holder (Fig. 4). The samples were arranged in a circle, with sample A in the centre thus receiving more irradiance and samples B and C at the edge. In order to fit all samples in the test array, the samples were cut smaller (7 cm × 7 cm). The set-point of the climate chamber's maximum temperature was raised back to 100 °C (Fig. 5). The UV and total irradiance values during phases 1–3 for samples A–C are shown in Table 1.

3.4. Constant temperature testing at 120 and 180 °C without irradiance

Reference tests were performed at 120 and 180 °C (stagnation temperature) for determining the effect of constant temperature alone on the optical properties. Unaged samples A–C were used for these tests. Test at 120 °C was performed in the climate chamber and the test at 180 °C was performed with an air-circulating oven. Absorptance and emittance of the samples were measured as new and after completing the tests after 735 and 550 h, respectively. Intermediate measurements of α were performed after 144 h for the 120 °C test and after 190 and 360 h for the 180 °C test.

4. Results

4.1. Cumulative UV irradiation after the three phases of the temperature and irradiance cycling test

We compared the UV stress within the climate chamber to the natural UV stress, i.e. the equivalent natural UV irradiation time in years. Bird and Hulström [18] have calculated solar direct normal UV radiation and Feisner and Grasnick [19] have measured solar global UV radiation. Both reported solar UV irradiance levels of 2.5–5.2% of the solar global irradiance. Based on this information, we calculated the corresponding UV stress coefficients for UV levels of 3–6% of the solar global irradiance (Table 2). In this case the solar global irradiation is estimated to be 4280 MJ/year, typical in Northern Europe. In total, sample A and samples B and C were exposed to radiant UV exposure equivalent to 7–15 and 5–10 years of normal operation, respectively, depending on the geographical location of the

Table 2
Calculated total UV exposure levels during temperature and irradiance cycling inside the climate chamber for phases 1–3 compared with equivalent solar global UV irradiation. Results for samples A–C

	Days of exposure in climate chamber	Total UV irradiation from UV-lamps (MJ)	Average equivalent years of UV irradiation for certain exposure times and UV/G ratios compared with solar global UV irradiation level per year[a]			
			UV/G = 3%	UV/G = 4%	UV/G = 5%	UV/G = 6%
Phase 1, samples A–C	100	16	0.12	0.09	0.07	0.06
Phase 2, samples A–C	150	390	3.0	2.2	1.8	1.5
Phase 3, sample A	133	1500	12	8.7	7.2	5.8
Phase 3, samples B and C	133	900	7.0	5.2	4.3	3.6
Total, sample A	383	1900	15	11	9.0	7.4
Total, samples B and C	383	1300	10	7.4	6.1	5.0

[a] Reference solar global irradiation (G) is 4280 MJ/year.

comparison area. However, the spectral radiation flux of the UV-lamps is not evenly distributed [20]. It has remarkably high peaks at certain wavelengths, e.g. near 370 nm. This has to be noted if the samples are especially sensitive to some part of the UV spectrum.

4.2. Changes in optical properties due to cycling and irradiance exposure

The most noticeable changes were measured in the solar absorptance. The first 50 days of temperature and irradiance cycling of samples A, B and C had a clear positive effect on α, which increased from 0.82, 0.81 and 0.86 to 0.86, 0.87 and 0.89, respectively (Fig. 6). Figs. 7–9 show the spectral hemispherical reflectance, ρ_λ, of samples A–C from 0.3 to 20 μm as new and after the 383 days of cycling. ρ_λ of samples A and B changed somewhat similarly, increasing slightly at shorter wavelengths (between 0.3 and 0.4 μm) and decreasing significantly at around 0.5–7 μm. For sample C, changes were similar but smaller. Further tests at a constant temperature of 120 and 180 °C confirm that elevated temperature alone can cause similar changes. A possible explanation for the changes of α is thermal induced relaxation of surface tension that remained due to the mechanical manufacturing in the surface lattice structure. Changes in the spectral reflectance after cycling can be due to changes in the surface topology (graphite cluster thickness, periodicity, etc.) as well.

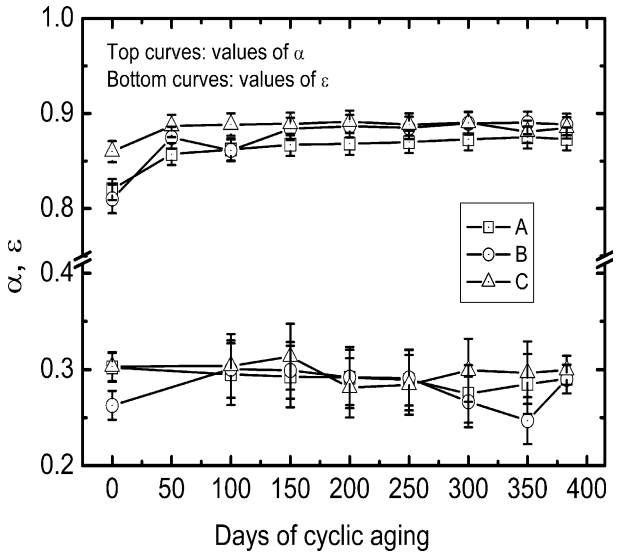

Fig. 6. Total hemispherical absorptance α and total hemispherical emittance ε of samples A–C as new, after each period of 50 days, and after 383 days in climate chamber. Reliable emittance data after 50 days are missing. Values as new and after 383 days are verified by Uppsala University; all intermediate values were measured at the Helsinki University of Technology only.

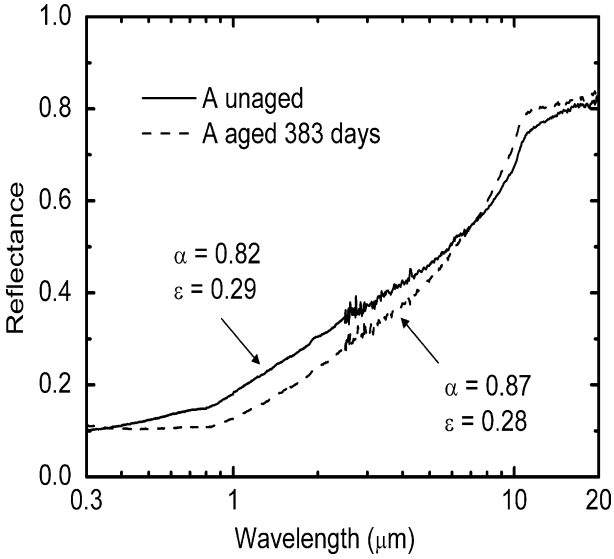

Fig. 7. Reflectance of sample A unaged and after 383 days of temperature and irradiance cycling in the climate chamber. Solar absorptance and thermal emittance before and after aging.

The smaller changes of α for sample C can be due to the different manufacturing procedures: after grinding, samples A and B were subjected to an acid bath containing potassium permanganate, cupric nitrate and nitric acid, whereas sample C

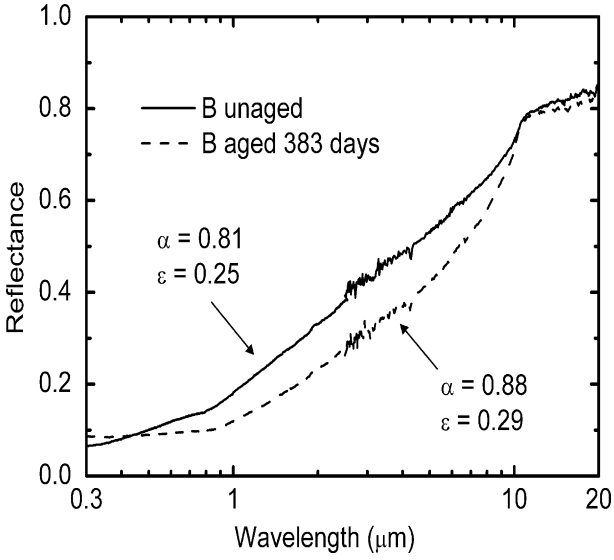

Fig. 8. Reflectance of sample B unaged and after 383 days of temperature and irradiance cycling in climate chamber. Solar absorptance and thermal emittance before and after aging.

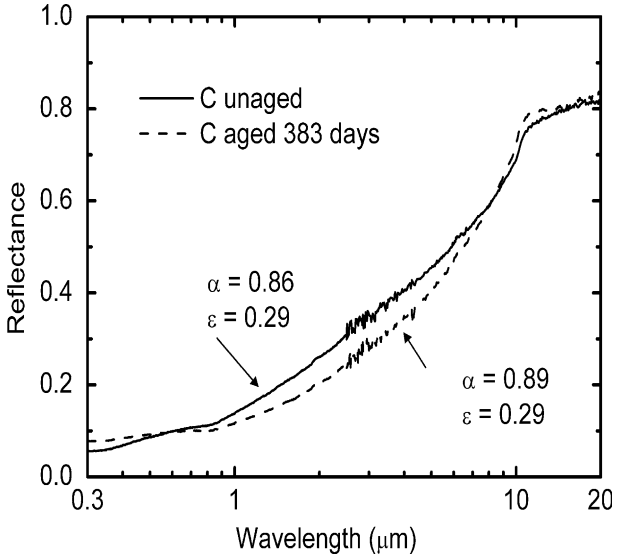

Fig. 9. Reflectance of sample C unaged and after 383 days of temperature and irradiance cycling in climate chamber. Solar absorptance and thermal emittance before and after aging.

was only ground (see [1] for details). It is likely that acids adsorbed onto the surface structure of samples A and B evaporate either partially or completely during heating to 120 °C thus changing the optical properties of surfaces A and B more compared to C.

According to Köhl [7], most of the absorber coatings have no sensitivity to UV, since they consist of inorganic materials. Although these surfaces consist of a graphite/Al_2O_3 surface matrix structure [2], they showed no degradation of α due to UV irradiation during the whole test period, i.e. no sensitivity to natural levels of UV was observed. The biggest changes in α occurred during the first 50 days, when the total maximum measured irradiance levels were 730–840 W m^{-2}, and the UV irradiance was negligible (Table 1). Absorptance of all the samples stabilized after the first 50 days, since the additional 333 days of aging had very little effect on α of any of the samples within the measuring accuracy. However, the spectral reflectance curves are somewhat flatter throughout the whole Vis–NIR spectrum after 250 days of cycling (383 days for sample A) compared to that after 100 days of cycling (Fig. 10). This indicates that strong UV or UV–Vis–IR exposure changes the spectral absorptance α_λ, but does not lower the integrated α, and therefore has no significant effect on the energy yield of the surface. According to McKenzie [13], metal atoms are capable of diffusing into the graphite and establishing a concentration of metal both in the graphite and on its surface, thus causing changes in the spectral reflectance. McKenzie's results are based on tests at temperatures of 200–500 °C. It is uncertain whether a temperature of 130 °C combined with high irradiance is sufficient to cause similar diffusion.

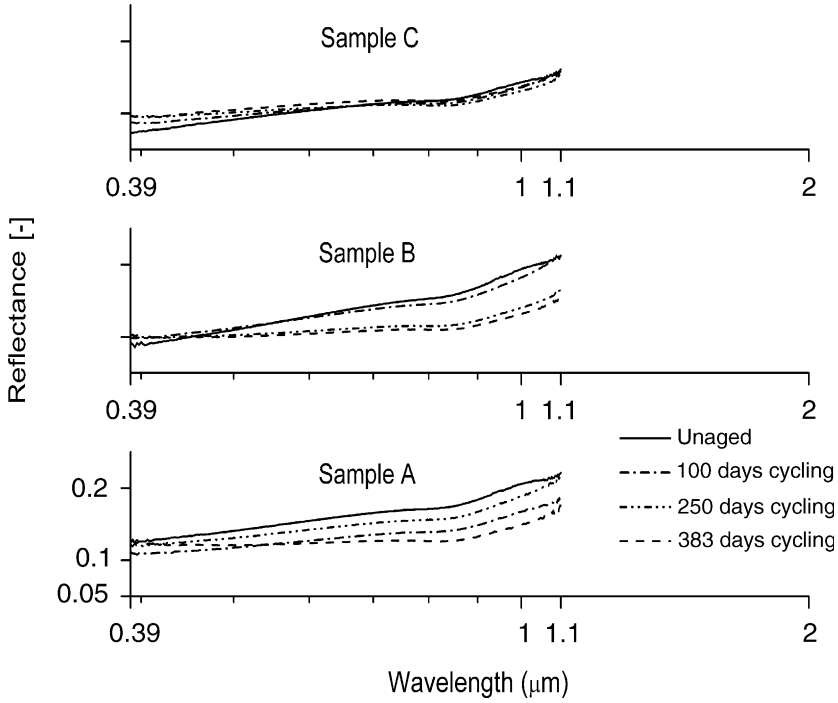

Fig. 10. Spectral reflectance of samples A–C in the Vis–NIR region, unaged and after 100, 250 and 383 days of temperature and irradiance cycling. Measured between 0.39 and 1.1 μm with a Li-cor 1800 spectroradiometer.

The emittances of samples A, B and C were 0.29, 0.25 and 0.29 before the cycling tests and 0.29, 0.29 and 0.30 after the tests, respectively, all values based on the Uppsala measurements. Emittance of the samples A and C did not change significantly during the 383 day test period. Emittance of sample B increased from 0.25 to 0.29. Again, evaporation of chemical residues can explain the change. It is not known why a similar change did not occur for the acidulated sample A. However, ε of sample B, being initially smaller, converged closer to the other samples after the tests. The deviation in the results can be caused by sample inhomogeneity as well as measurement accuracy. Differences in ε were observed for all the samples between almost every test period of 50 days, but the differences are within the estimated measurement error limit.

4.3. Changes in optical properties after constant temperature testing at 120 and 180 °C without irradiance

A small increment in α was determined as a result of the exposure to constant temperature at 120 and 180 °C for all samples A–C (Table 3). The change of α for sample C is smaller in most cases, probably due to the same reason as in the 383

Table 3
Changes in solar absorptance and thermal emittance for samples A–C due to constant temperature thermal aging at 120 and 180 °C. Sample D is from a solar collector that has been in operation for 4 years. α was measured between 0.39 and 1.1 μm with a Li-cor 1800 spectroradiometer and ε was measured between 2.5 and 20 μm with a Midac FTIR spectrometer

	Solar absorptance α					Thermal emittance ε				
	As new	After 735 h at 120 °C	Change 735 h at 120 °C	After 550 h at 180 °C	Change 550 h at 180 °C	As new	After 735 h at 120 °C	Change 735 h at 120 °C	After 550 h at 180 °C	Change 550 h at 180 °C
Sample A	0.84	0.85	0.01	0.87	0.03	0.34	0.36	0.02	0.32	−0.02
Sample B	0.85	0.87	0.02	0.86	0.01	0.29	0.30	0.01	0.28	−0.01
Sample C	0.88	0.89	0.01	0.89	0.01	0.33	0.34	0.00	0.33	0.00
Sample D	0.89 (after 4 years of natural exposure)					0.31 (after 4 years of natural exposure)				

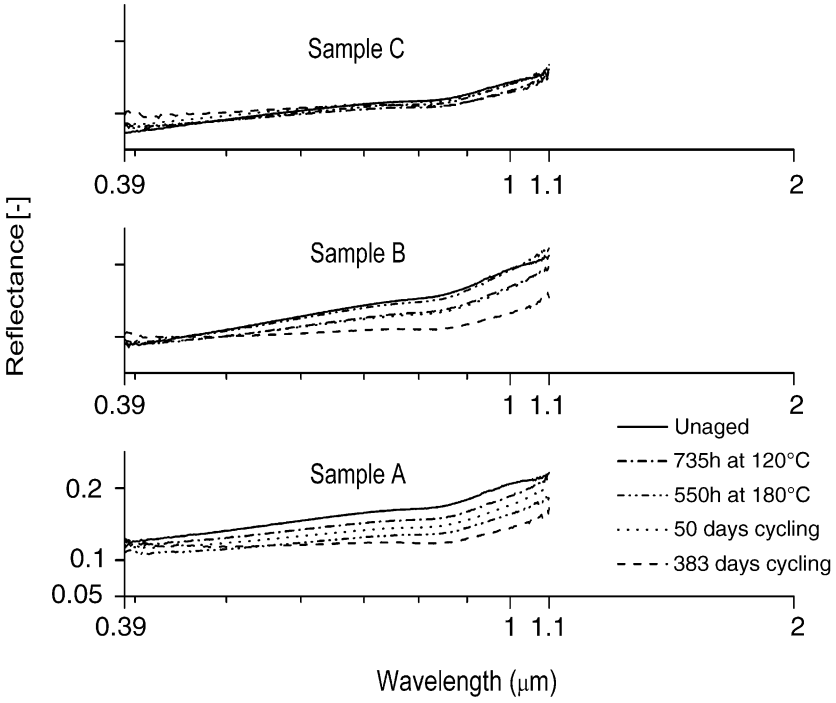

Fig. 11. Spectral reflectance of samples A–C in the Vis–NIR region, unaged and after constant temperature test at 120 and 180 °C, compared to 50 and 383 days of temperature and irradiance cycling. Measured between 0.39 and 1.1 μm with a Li-cor 1800 spectroradiometer.

days cycling test. The shape of the reflectance diagrams between 0.39 and 1.1 μm as new and after 120 and 180 °C test is close to that after the first 50 days of cycling (Fig. 11). Again, the deviation in the results can be caused by sample inhomogeneity and measurement accuracy. Absolute changes in ε were within ± 0.02, thus remaining within the measurement accuracy.

Intermediate measurements of α after 190 and 360 h for the 180 °C test showed that no additional changes occurred after the first 190 h at 180 °C. Small additional changes in α were determined between the intermediate 144 h and final 120 °C measurements.

5. Discussion

Thermal cycling between −40 and 120 °C combined with irradiance load deepened the understanding of the aging response of mechanically manufactured selective $C/Al_2O_3/Al$ absorber samples, especially regarding improvement of the solar absorptance. The standard IEA SHC tests [6–9] (200 h at 250 °C) do not provide any information about the UV induced degradation, or—in this case—the

conditions needed for the improvement of α. The cycling method simulates the natural exposure to some extent, and here supplements the standard tests suggested by the IEA SHC.

A reference surface denoted D was disassembled from a solar collector, which has been at our testing facility in Espoo (60° 11′ N, 24° 50′ E, collector south-oriented, and slope 53°) for 4 years, mostly in stagnation without fluid circulation. Unfortunately, α and ε of the surface D as new are unknown. Most likely they were in the same range with samples A and B because of the same manufacturing period and methodology. After natural exposure, both α and ε of sample D (average of three samples taken from the collector, see Table 3) are very close to those of samples A and B after 383 days of cycling. Thus, it seems that the same mechanism(s), which cause the increase in α and ε during accelerated aging cycling occur in nature as well. It is likely that the observed increment in absorptance will occur in normal use after a short period of time, after a collector is exposed to solar radiation.

6. Conclusions

Efforts should be made in order to optimize the composition of the grinding pad and adjust the grinding parameters accordingly to produce surfaces which could take further advantage of surface plasmons. Commercially available grinding pads tested so far does not seem to be optimal for manufacturing the surface. Theoretically, with optimal graphite thickness, groove depth and surface periodicity, emittance could be significantly lowered. By adding an antireflection coating such as low-cost colloidal silica dipping, the optimized surface could have $\alpha > 0.90$ with ε unaffected.

Mechanically manufactured selective $C/Al_2O_3/Al$ absorber surface samples were subjected to 383 days of combined temperature and irradiance cycling within the temperature range of -40 to 120 $^\circ$C and UV–Vis–IR irradiance of 1000–7000 W m^{-2}. α increased significantly and ε remained unchanged for the majority of the samples. The biggest change in α occurred after the first 50 days of aging with negligible UV levels. Constant temperature tests after a few hundred hours at 120 and 180 $^\circ$C showed similar changes in α. Increasing the total and UV irradiance during the cyclic test changed α_λ slightly without lowering α. Similar values of α and ε were measured for test site samples after 4 years of natural exposure and for samples after 383 days of cycling, thus indicating corresponding aging behaviour in both cases.

Acknowledgements

Support by the Finnish National Technology Agency (TEKES) is gratefully acknowledged. We would also like to thank Dr. Tuquabo Tesfamichael from the Ångström Laboratory of Uppsala University for the optical reference measurements.

References

[1] Konttinen P, Lund PD, Kilpi R. Mechanically manufactured selective solar absorber surfaces. Solar Energy Mater Solar Cells 2003;79(3):273–83.

[2] Konttinen P, Kilpi R, Lund PD. Microstructural analysis of selective $C/Al_2O_3/Al$ solar absorber surfaces. Thin Solid Films 2003;425(1–2):24–30.

[3] Botten LC, Ritchie IT. Improvements in the design of solar selective thin film absorbers. Opt Commun 1977;23:421–6.

[4] Golomb M. Diffraction gratings and solar selective thin film absorbers: an experimental study. Opt Commun 1978;27:177–80.

[5] Kudryashova MD. Mechanical treatment of collector surfaces in solar installations leading to improved selectivity of optical properties. Appl Solar Energy 1969;5:24–5.

[6] Carlsson B, Frei U, Köhl M, Möller K. Accelerated life testing of solar energy materials—case study of some selective materials for DHW-systems. IEA SHCP Task X; 1994.

[7] Köhl M. Durability of solar energy materials. Renew Energy 2001;24(3–4):597–607.

[8] Carlsson B, Möller K, Köhl M, Frei U, Brunold S. Qualification test procedure for solar absorber surface durability. Solar Energy Mater Solar Cells 2000;61(3):255–75.

[9] Brunold S, Frei U, Carlsson B, Möller K, Köhl M. Accelerated life testing of solar absorber coatings: testing procedure and results. Solar Energy 2000;68(4):313–23.

[10] Konttinen P, Lund PD. Thermal stability and moisture resistance of $C/Al_2O_3/Al$ solar absorber surfaces. Solar Energy Mater Solar Cells [in press].

[11] Raether H. Surface plasmons on smooth and rough surfaces and on gratings. Berlin: Springer-Verlag; 1988.

[12] Wood RH. Anomalous diffraction gratings. Phys Rev 1935;48:928–36.

[13] McKenzie DR. Effect of substrate on graphite and other solar selective surfaces. Appl Opt 1978;17:1884–8.

[14] Nostell P, Roos A, Karlsson B. Optical and mechanical properties of sol–gel antireflective films for solar energy applications. Thin Solid Films 1999;351:170–5.

[15] Konttinen P. Accelerated aging and optical characterization of absorber surfaces for solar collectors. Licentiates Thesis. Helsinki University of Technology, 2000. Available from: http://www.hut.fi/Units/AES/studies/theses/konttine.pdf.

[16] Wan T, Zhao Q, Cheng X. Preparation process and property analysis of a solar selective absorbing surface on milled steel. Solar Energy Mater Solar Cells 1993;30(4):285–90.

[17] Carlsson B, editor. Survey of service prediction methods for materials in solar heating and cooling. International Energy Agency Solar Heating and Cooling Programme Task X: Solar Materials Research and Development. Document D16:1989. Stockholm, Sweden: Swedish Council for Building Research.

[18] Bird RE, Hulström RL. Terrestrial solar spectral data sets. Solar Energy 1983;30(6):563–73.

[19] Feisner U, Grasnick KH. Solar UV radiation measurements at Potsdam (52° 22′ N, 13° 5′ E). Solar Energy 1992;49(6):541–8.

[20] OSRAM. Special lamps from OSRAM for technical applications. AB 451/890, p. 10–11.